# HI Fluctuations at Large Redshifts: III – Simulating the Signal Expected at GMRT

Somnath Bharadwaj* & Pennathur Sridharan Srikant[†]
*Department of Physics and Meteorology and Center for Theoretical Studies, I.I.T. Kharagpur, 721 302, India.
e-mail: somnath@phy.iitkgp.ernet.in
[†]Department of Physics and Meteorology, I.I.T. Kharagpur, 721 302, India.
[†]Present address: Department of Physics, University of Utah, USA.

**Abstract.** We simulate the distribution of neutral hydrogen (HI) at the redshifts $z = 1.3$ and 3.4 using a cosmological N-body simulation along with a prescription for assigning HI masses to the particles. The HI is distributed in clouds whose properties are consistent with those of the damped Lyman-$\alpha$ absorption systems (DLAs) seen in quasar spectra. The clustering properties of these clouds are identical to those of the dark matter. We use this to simulate the redshifted HI emission expected at 610 MHz and 325 MHz, two of the observing bands at the GMRT. These are used to predict the correlations expected between the complex visibilities measured at different baselines and frequencies in radio-interferometric observations with the GMRT. The visibility correlations directly probe the power spectrum of HI fluctuations at the epoch when the HI emission originated, and this holds the possibility of using HI observations to study large-scale structures at high $z$.

*Key words.* Cosmology: theory, observations, large scale structures— radiation.

## 1. Introduction

Observations of Lyman-$\alpha$ absorption lines seen in quasar spectra are an important probe of the distribution of neutral hydrogen (HI) at high redshifts. These observations show that the bulk of the neutral gas in the redshift range $1 \leq z \leq 3.5$ is in HI clouds with column densities greater than $2 \times 10^{20}$ atoms/cm$^2$ (Lanzetta *et al.* 1995; Storrie-Lombardi *et al.* 1996; Péroux *et al.* 2001). The damped Lyman-$\alpha$ absorption lines produced by these clouds indicate $\Omega_{gas}(z)$, the comoving density of neutral gas expressed as a fraction of the present critical density, to be nearly constant at a value $\Omega_{gas}(z) \sim 10^{-3}$ (Péroux *et al.* 2001).

In this paper we simulate the HI emission expected from these clouds. The aim of the exercise is to investigate the possibility of detecting the redshifted HI emission using the Giant Meterwave Radio Telescope (GMRT; Swarup *et al.* 1991). We focus on two of the GMRT frequency bands centered at 610 MHz and 325 MHz corresponding to HI

emission from redshifts $z = 1.3$ and $3.4$. The HI flux from individual clouds ($< 10\mu$Jy) is too weak to be detected by GMRT unless the image of the cloud is significantly magnified by an intervening cluster gravitational lens (Saini *et al.* 2001). Although we may not be able to detect individual clouds, the redshifted HI emission from the distribution of clouds will appear as a background radiation in low frequency radio observations. In three earlier papers (Bharadwaj *et al.* 2001; Bharadwaj & Sethi 2001 and Bharadwaj & Pandey 2003; hereafter referred to as Paper a, b and c respectively), and in the present paper we investigate issues related to calculating the expected signal and detecting it.

We propose (Papers b and c) that the optimal observational strategy for detecting this signal is to deal directly with the complex visibilities measured in radio interferometric observations. Briefly introducing the terms involved, we remind the reader that the quantity measured in radio interferometric observations with an array of antennas is the complex visibility $V(\mathbf{U}, \nu)$. This is measured for every pair of antennas at every frequency channel in the observation band. For every pair of antennas it is convenient to express the visibility as a function of $\mathbf{U} = \mathbf{d}/\lambda$ i.e., the separation between the two antennas $\mathbf{d}$ expressed in units of the wavelength $\lambda$. We refer to the different possible values of $\mathbf{U}$ as baselines. One of the big advantages of dealing directly with the visibilities is that the system noise contribution to the visibilities is uncorrelated. The visibilities respond only to the fluctuations in the redshifted HI emission. In Paper b we showed that the correlation expected between the visibilities $V(\mathbf{U}, \nu)$ and $V(\mathbf{U}, \nu + \Delta\nu)$ measured at the same baseline at two slightly different frequencies is

$$\langle V(\mathbf{U}, \nu)V^*(\mathbf{U}, \nu + \Delta\nu)\rangle = \frac{[\bar{I}bD\theta_0]^2}{2r^2} \int_0^\infty dk_\parallel P(k) \left[1 + \beta\frac{k_\parallel^2}{k^2}\right]^2 \cos(k_\parallel r'\Delta\nu), \quad (1)$$

where $k = \sqrt{(2\pi U/r)^2 + k_\parallel^2}$, $\bar{I}_0$ is the specific intensity expected from the HI emission if the HI were uniformly distributed, $\theta_0 = 0.6 \times \theta_{\mathrm{FWHM}}$, $\theta_{\mathrm{FWHM}}$ being the angular width of the primary beam of the individual antennas, $r$ is the comoving distance to the HI from which the radiation originated, and $b^2 D^2 P(k) \left[1 + \beta\frac{k_\parallel^2}{k^2}\right]^2$ is the power spectrum of the fluctuations in the HI distribution in redshift space at the epoch when the HI emission originated.

To summarize, the visibility-visibility cross-correlation (hereafter refereed to as the visibility correlation) directly probes the power spectrum of HI fluctuations at the epoch where the HI emission originated. This holds the possibility of allowing us to study the large scale structures at high redshifts. A point to note is that the visibility correlations at a baseline $U$ receives contribution from the power spectrum only for Fourier mode $k > k_{\mathrm{min}} = (2\pi/r)U$, and for the CDM-like power spectrum most of the contribution comes from Fourier modes around $k_{\mathrm{min}}$. So, it may be said that the correlations at a baseline $U$ probes the power spectrum at the Fourier mode $(2\pi/r)U$.

In the earlier work we treated the HI as being continuously distributed whereas in reality the HI resides in discrete gas clouds. In addition, it was assumed that the HI distribution is an unbiased representation of the underlying dark matter distribution, and we used the linear theory of density perturbations to follow the evolution of fluctuations in the dark matter distribution. It is these assumptions which allow us to express the power spectrum of fluctuations in the HI distribution in redshift space at the epoch when the HI emission originated (in equation 1) in terms of $b$ the linear

bias parameter (taken to be 1), $D$ the growing mode of linear density perturbations (Peebles 1980) at the epoch when the HI emission originated, $P(k)$ the present power spectrum of dark matter density fluctuations calculated using linear theory and the factor $\left[1 + \beta \frac{k_{\parallel}^2}{k^2}\right]^2$ which takes the power spectrum from real space to redshift space in the linear theory of redshift distortions (Kaiser 1987). Here we report progress on two counts. First, we have used a PM N-body code to evolve the fluctuations in the dark matter distribution, thereby incorporating possible non-linear effects. Second, we have assigned HI masses to the dark matter particles in the N-body code and this was used to simulate the redshifted HI emission. So we have also been able to incorporate the fact that the HI gas is contained in discrete clouds. The predictions for the HI signal expected at GMRT presented in this paper incorporate both these effects. We still retain the assumption that the HI is an unbiased tracer of the dark matter.

We next present a brief outline of this paper. In section 2 we discuss the method that was used to simulate the HI signal, and in section 3. we present the results of our investigations. In section 4 we discuss the results and present conclusions.

Finally, it should be pointed out that there have been alternative lines of approach investigating the possibility of using HI observations to study large scale structures at $z \sim 3$ (Sunyaev & Zeldovich 1975; Subramanian & Padmanabhan 1993; Kumar *et al.* 1995; Weinberg *et al.* 1996; Bagla *et al.* 1997; Bagla & White 2002). The reader is referred to Papers a and b for a detailed comparison of these approaches with that adopted here.

## 2. Methodology

We have simulated the visibility correlations expected at two of the GMRT observing frequency bands centered at $\nu_c = 610\,\text{MHz}$ and $325\,\text{MHz}$. The simulations were carried out in three steps:

- Using a PM N-body code to simulate the dark matter distribution at the redshift where the HI emission originated
- Assigning HI masses to the particles used in the N-body code and calculating the flux expected from each HI cloud
- Calculating the complex visibilities arising from the distribution of HI clouds and computing the visibility correlations.

We next discuss the salient features of each of these steps. The values $h = 0.7$, $\Omega_{m0} = 0.3$ and $\Omega_{\Lambda 0} = 0.7$ were used throughout.

### 2.1 *The N-body simulations*

We have used a Particle-Mesh (PM) N-body code to simulate the dark matter distribution at the redshift $z$ where the HI emission originated. The simulation volume was a cubic box of comoving volume $L^3$. The size $L$ was chosen so that it is approximately twice the comoving distance subtended by $\theta_{\text{FWHM}}$ of the GMRT primary beam.

The values of $r$ the comoving distance to the region from where the HI emission originated, the grid spacing of the mesh $\Delta L$, and the number of dark matter particles used in each simulation $N_{\text{DM}}$ are all shown in table 1.

**Table 1.**

| $v_c$ (MHz) | $z$ | $\theta_{FWHM}$ | $r$ (Mpc) | $L$ (Mpc) | $\Delta L$ (Mpc) | $N_{DM}$ | $N_{SIM}$ | $z_{in}$ |
|---|---|---|---|---|---|---|---|---|
| 610 | 1.33 | 0.9° | 4030 | 128 | 0.5 | $128^3$ | 4 | 19 |
| 325 | 3.37 | 1.8° | 6686 | 512 | 1 | $256^3$ | 4 | 9 |

The initial power spectrum of dark matter density fluctuations at $z_{in}$ (shown in table 1) is normalized to COBE (Bunn & White 1996), and its shape is determined using the analytic fitting form for the CDM power spectrum given by Efstathiou *et al.* (1992). The value of the shape parameter turns out to be $\Gamma = 0.2$ for the set of cosmological parameters used here. We have run the N-body code for $N_{SIM}$ (table 1) independent realisations of the initial conditions and the final results for the visibility correlations were averaged over all the realisations.

The N-body code gives the final positions and peculiar velocities of the $N_{DM}$ dark matter particles in the simulation. The power spectrum of the density fluctuations in the dark matter distribution at $z = 1.33$ and $z = 3.37$ is shown in Figs. 1 and 2 respectively. In both the figures we have shown the power spectrum for the range of Fourier modes which will make a significant contribution to the visibility correlation at the baselines where the signal is expected to be strongest. We find that at $z = 1.33$ (610 MHz) the power spectrum obtained from the N-body simulation shows
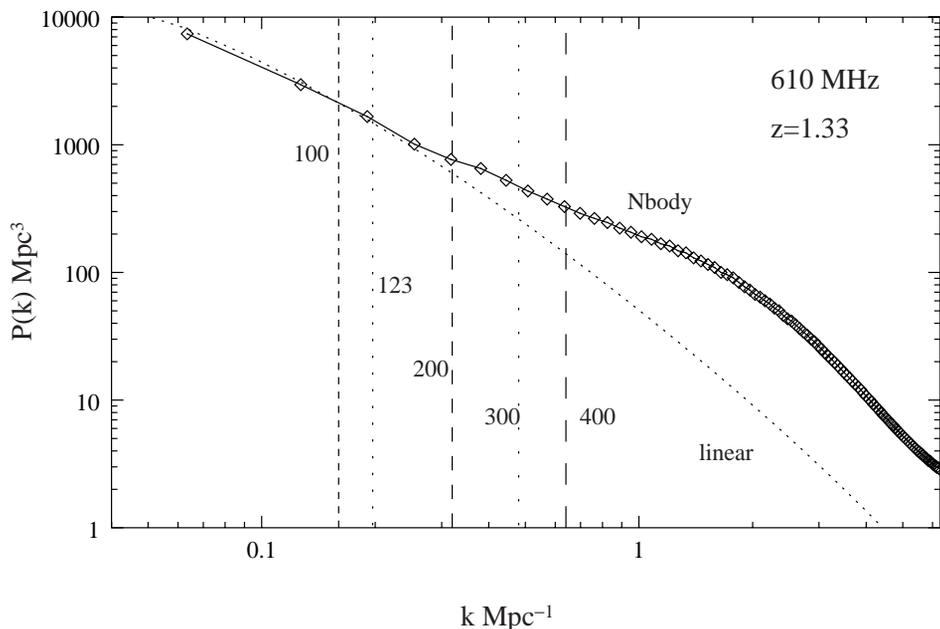


**Figure 1.** This shows the power spectrum of density fluctuations in the dark matter distribution at $z = 1.33$. The vertical lines show the smallest Fourier mode $k_{min} = (2\pi/r)U$ which contributes to the visibility correlations at a baseline $U$. This is shown for the different values of $U$ indicated in the figure.
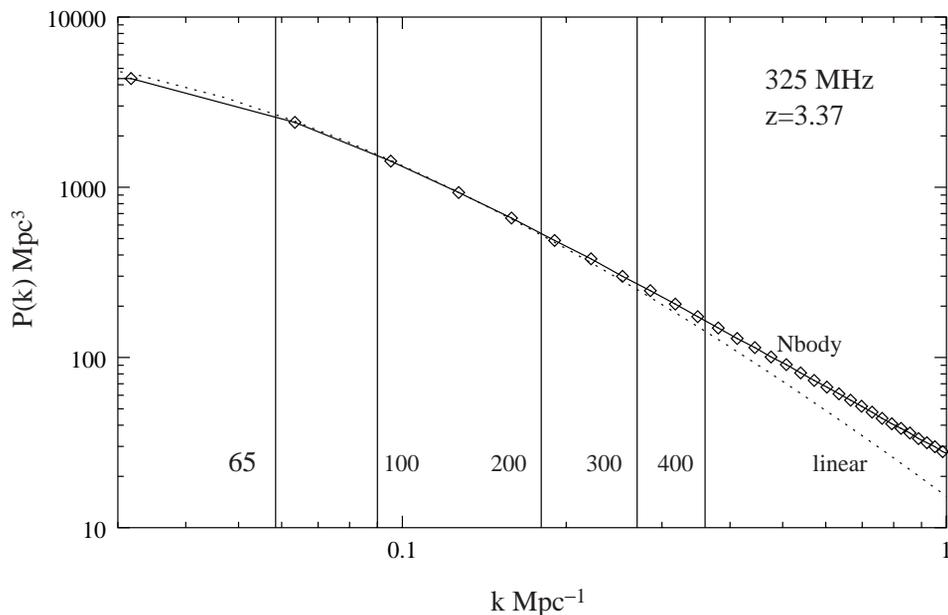
**Figure 2.** This is the same as Fig. 1 except that it is at $z = 3.37$ which corresponds to 325 MHz.

substantial differences from the power spectrum calculated using linear theory at Fourier modes $k \geq 0.3 \, \mathrm{Mpc}^{-1}$. Converting to baselines, we expect non-linear effects to be important for $U \geq 200$. At $z = 3.37 \, (325 \, \mathrm{MHz})$ there are differences between the N-body and linear power spectrum at $k \geq 0.3 \, \mathrm{Mpc}^{-1}$, but the non-linear effects are not as pronounced as at 610 MHz. Converting to baselines, non-linear effects will influence the signal at baselines $U \geq 400$.

## 2.2 *Assigning HI masses*

We model the HI clouds as randomly oriented rotating disks of radius $R$, column density $N_{\mathrm{HI}}$ and rotation velocity $V$. The values of $R$ and $V$ are held fixed in each simulation, and we have run simulations with different sets of values for these parameters. It is assumed that the column densities have a power law distribution in the range $2 \times 10^{20} \leq N_{\mathrm{HI}}/(\mathrm{atoms/cm}^2) \leq 1 \times 10^{22}$ and the comoving number density of HI clouds with column densities in the interval $dN_{\mathrm{HI}}$ is $B N_{\mathrm{HI}}^{-\alpha} \, dN_{\mathrm{HI}}$. The total comoving number density of HI clouds at redshift $z$ is

$$n_{\mathrm{HI}}^{c}(z) = B \int_{N_{\mathrm{HI}}[\mathrm{min}]}^{N_{\mathrm{HI}}[\mathrm{max}]} N_{\mathrm{HI}}^{-\alpha} \, dN_{\mathrm{HI}} \qquad (2)$$

and the comoving mass density is

$$\rho_{\mathrm{HI}}^{c}(z) = B \int_{N_{\mathrm{HI}}[\mathrm{min}]}^{N_{\mathrm{HI}}[\mathrm{max}]} (\pi R^2 N_{\mathrm{HI}} m_{\mathrm{HI}}) N_{\mathrm{HI}}^{-\alpha} \, dN_{\mathrm{HI}}, \qquad (3)$$

where $m_{HI}$ is the mass of the hydrogen atom. The normalisation coefficient $B$ is determined by using equation (3) to calculate $\Omega_{gas}(z)$

$$\Omega_{gas}(z) = \frac{4}{3}\Omega_{HI}(z) = \frac{4}{3}\frac{8\pi G}{3H_0^2}\rho_{HI}^c(z). \tag{4}$$

We use $\Omega_{gas} = 10^{-3}$ in all the simulations.

This model fixes the total number of HI clouds in the simulation volume $N_{clouds} = L^3 n_{HI}^c(z)$ . The total number of clouds scale as

$$N_{clouds} \propto \frac{1-\alpha}{2-\alpha}R^{-2}, \tag{5}$$

as we vary $\alpha$ the slope of the column density distribution or the radius of the clouds $R$. For large values of $R$ the HI is distributed in a few clouds with large masses, whereas there are many clouds with low HI masses when $R$ is small. Our model has three free parameters, namely $\alpha$, $R$ and $V$. We have run simulations varying $\alpha$ and $R$ (table 2) for $V = 100\,\text{km/s}$ and $200\,\text{km/s}$.

We randomly select $N_{clouds}$ particles from the output of the N-body simulation and these are identified as HI clouds. The HI mass of each cloud is $M_{HI} = \pi R^2 N_{HI} m_{HI}$, where the column density is drawn randomly from the power-law distribution discussed earlier. The center of the simulation volume is aligned with the center of the GMRT primary beam and it is located at a comoving distance corresponding to the redshift $z$. The comoving distance to each cloud is used to calculate its angular position and redshift. The redshift is used to determine the luminosity distance which is used to calculate the flux from the individual clouds. The effect of the peculiar velocity is incorporated when calculating $\nu_o$ the frequency at which the HI emission from each

**Table 2.**

| $\nu_c$ (MHz) | $\alpha$ | $R$ Kpc | $n_{HI}^c(z)$ Mpc$^{-3}$ | $N_{clouds}$ |
|---|---|---|---|---|
| 610 | 1.2 | 10 | $2.0 \times 10^{-2}$ | 42467 |
| 610 | 1.2 | 8 | $3.2 \times 10^{-2}$ | 66354 |
| 610 | 1.2 | 5 | $8.1 \times 10^{-2}$ | 169865 |
| 610 | 1.2 | 2 | $5.1 \times 10^{-1}$ | 1061651 |
| 610 | 1.7 | 10 | $3.7 \times 10^{-2}$ | 76764 |
| 610 | 1.7 | 8 | $5.7 \times 10^{-2}$ | 119943 |
| 610 | 1.7 | 5 | $1.5 \times 10^{-1}$ | 307055 |
| 610 | 1.7 | 2 | $9.2 \times 10^{-1}$ | 1919088 |
| 325 | 0.8 | 10 | $1.3 \times 10^{-2}$ | 1799234 |
| 325 | 1.2 | 10 | $2.0 \times 10^{-2}$ | 2717825 |
| 325 | 1.2 | 8 | $3.2 \times 10^{-2}$ | 4246602 |
| 325 | 1.2 | 5 | $8.1 \times 10^{-2}$ | 10871300 |

cloud is received. The line width $\Delta \nu$ of the HI emission line from each cloud is calculated using $\Delta \nu = \mid \sin \theta \mid 2 \nu_o V / c$, where $2 \nu_o V / c$ is the line width if the disk of the galaxy were viewed edge on and $\theta$ is the angle between the normal to the disk and the line of sight.

To summarize, at the end of this stage of the simulation we have $N_{\text{clouds}}$ HI clouds. For each cloud we have its angular position $\vec{\theta}^a$, and the flux density $F^a$, frequency $\nu_o^a$ and line-width $\Delta \nu^a$ of the redshifted HI emission. Here the index $a$ ($1 \leq a \leq N_{\text{clouds}}$) refers to the different clouds in the simulation.

## 2.3 *Calculating visibility correlations*

We first describe how we have calculated the complex visibilities that would be measured in GMRT radio observations of the HI distribution generated in the simulation. The observations are carried out at $NC$ frequency channels $\{\nu_1, \nu_2, \nu_3, \dots, \nu_{NC}\}$ covering a frequency band $B$ centered at the frequency $\nu_c$. We have used $B = 8\,\text{MHz}$ and $NC = 64$ at $\nu_c = 610\,\text{MHz}$, and $B = 8\,\text{MHz}$ and $NC = 128$ at $\nu_c = 325\,\text{MHz}$.

For the purpose of this paper we assume that the antennas are distributed on a plane, and that they all point vertically upwards. The beam pattern $A(\vec{\theta})$ quantifies how the individual antenna, pointing upwards, responds to signals from different directions in the sky. This is assumed to be a Gaussian $A(\vec{\theta}) = e^{-\theta^2/\theta_0^2}$ where $\theta_0 = 0.6 \times \theta_{\text{FWHM}}$ (table 1).

The position of each antenna can be denoted by a two dimensional vector $\mathbf{d}_i$. The quantity measured in interferometric observations is the visibility $V(\mathbf{U}, \nu)$ which is recorded for every independent pair of antennas (baseline) at every frequency channel in the band. For any pair of antennas, the visibility depends on the vector $\mathbf{d} = \mathbf{d}_i - \mathbf{d}_j$ joining the position of the two antennas. It is convenient to express the visibility as a function of the variable $\mathbf{U}$ which is $\mathbf{d}$ expressed in units of the wavelength i.e., $\mathbf{U} = \mathbf{d}/\lambda$. The signal arising from the clustering pattern of the HI clouds will be strongest at the small baselines, and our calculations have been limited to this. We have considered a square grid of baselines extending from $-U_{\text{max}}$ to $U_{\text{max}}$ with resolution $\delta U$. We have used $U_{\text{max}} = 400$ and $\delta U = 10$. The complex visibility has been calculated for each baseline $\mathbf{U}$ on the grid using

$$V(\mathbf{U}, \nu) = \sum_{a=1}^{N_{\text{clouds}}} A(\vec{\theta}^a)\, F^a e^{-i2\pi \mathbf{U} \cdot \vec{\theta}^a}\, O\left(\frac{\mid \nu - \nu_o^a \mid}{\Delta \nu^a}\right), \qquad (6)$$

where the function $O(x)$ is defined such that $O(x) = 1$ for $x \leq 1$, else $O(x) = 0$. It is to be noted that in an actual GMRT observation the baselines will have a complicated distribution depending on which part of the sky is observed and the duration of the observation. Given the fact that the signal we are interested in is statistical in nature, and that we are interested in making generic predictions about the signal expected in a typical GMRT observation, a square grid of baselines is adequate.

The final step in the simulation is to calculate the visibility correlation $\langle V(\mathbf{U}, \nu) V^*$ $(\mathbf{U}, \nu + \Delta \nu)\rangle$. The angular brackets $\langle \rangle$ indicate the ensemble average, and we have averaged over the $N_{\text{SIM}}$ different realisation of the N-body simulation. In addition, the correlation depends only on the separation in frequency $\mid \Delta \nu \mid$, and the magnitude $U = \mid \mathbf{U} \mid$. So, for a fixed value of $\Delta \nu$ and $U$ we have averaged over all possible pairs of frequencies and baselines which match these values.

The analytic calculations (Papers b and c) where the HI is assumed to have a continuous distribution, predict the imaginary part of the visibility correlation function to be zero, and the clustering signal is manifest in only the real part. In the simulations we get a very small, but non-zero imaginary component. This is not discussed in the rest of the paper where we present results for the real component only.

## 3. Results

In this section we present results for the visibility correlation as obtained from our simulations. We compare these with the analytic predictions of Papers b and c and investigate the effect of two factors:

 (1)  the non-linear evolution of the density fluctuations, and
 (2)  the discrete nature of the HI distribution.

To get a better understanding of the second effect, we present results varying the parameters of the HI distribution.

### 3.1  *610 MHz*

Figure 3 shows the visibility correlations for $U = 100$, the results at smaller baselines show a similar behaviour. The visibility correlation at the baseline $U = 100$ receives
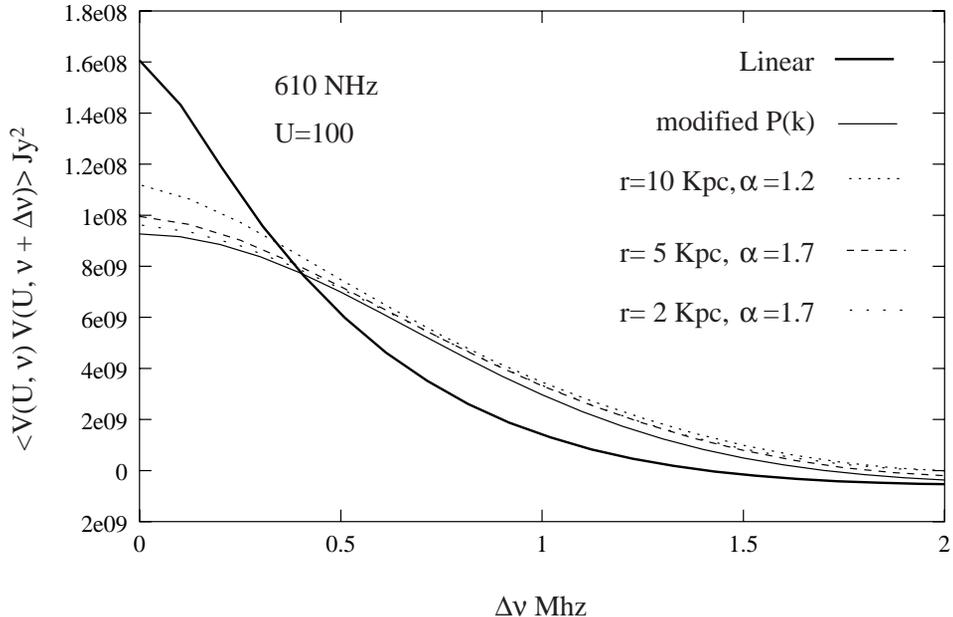


**Figure 3.**    This shows the correlation expected between the visibilities $V(\mathbf{U}, \nu)$ and $V(\mathbf{U}, \nu + \Delta\nu)$ at the same baselines at two different frequencies. The rotational velocity of the HI disk is assumed to be $V = 200$ km/s. The other parameters of the HI distribution take on values shown in the figure. These results are for the 610 MHz band.

contributions mainly from Fourier modes around $k \sim 0.2\,\mathrm{Mpc}^{-1}$ which is in the linear regime (Fig. 1), and we expect a good agreement with the analytic, linear predictions. We find that for $\Delta\nu < 0.5\mathrm{MHz}$ the analytic predictions are larger than the correlations obtained in the simulations, and this is reversed for $\Delta\nu > 0.5\,\mathrm{MHz}$. This discrepancy can be explained if we take into account the fact that visibility correlation actually responds to the clustering in redshift space. It is known (e.g., Suto & Suginohara 1991; Graman *et al.* 1993; Fisher *et al.* 1994; Brainerd *et al.* 1996; Bromley *et al.* 1997) that non-linear effects can be important in redshift space even on scales where the clustering in real space is well described by linear perturbation theory. It has been shown that this can be modeled by taking into account the effect of the random motions along the line of sight (e.g., Fisher *et al.* 1994; Peacock & Dodds 1994; Ballinger *et al.* 1996). We incorporate this by multiplying the power spectrum with $\exp[-k_{\parallel}^2 \sigma^2]$ in our analytic formulas for the visibility correlation. This gives the modified formula

$$\langle V(\mathbf{U}, \nu) V^*(\mathbf{U}, \nu + \Delta\nu) \rangle = \frac{[\bar{I} b D \theta_0]^2}{2r^2} \int_0^\infty dk_{\parallel} P(k) \left[ 1 + \beta \frac{k_{\parallel}^2}{k^2} \right]^2$$

$$\times \exp[-k_{\parallel}^2 \sigma^2] \cos(k_{\parallel} r' \Delta\nu) \qquad (7)$$

for the visibility correlation. We find that for $\sigma = 200\,\mathrm{km/s}/H_0$ this gives a good fit to the results of the simulations, and this is also shown in the figure. We next shift our attention to how the results depend on the parameters of the HI distribution. We find that for $r = 10\,\mathrm{Kpc}$ where the bulk of the HI is distributed in a few clouds with large HI masses the results show a 20% increment at small values of $\Delta\nu$ compared to the models with smaller values of $r$. This excess correlation at small $\Delta\nu$ arises from the fact that the HI emission from an individual cloud will be spread across a width $\delta\nu$ in frequency. The correlation between the HI emission from the same HI cloud at two different frequencies will contribute to the visibility correlations when $\Delta\nu \leq \delta\nu$. The contribution from this signal is significant in comparison to that arising from the clustering of the HI clouds when the total HI is distributed in a few clouds with large HI masses each. The contribution to the visibility correlation from within individual HI clouds goes down as $r$ is reduced and the HI is distributed among many clouds each with small HI masses. There is very little difference between the results for $r = 5\,\mathrm{Kpc}$ and $2\,\mathrm{Kpc}$ and we may treat this as the result if the HI were continuously distributed.

The results in Fig. 3 are for the rotational velocity $V = 200\,\mathrm{km/s}$. We have also done simulations using $V = 100\,\mathrm{km/s}$. We find that there are differences ($< 20\%$) only at small values of $\Delta\nu$. The effect of decreasing $V$ is to decrease the frequency width of the HI emission line from individual clouds which results in a higher value of the HI flux density. This does not effect the clustering signal but enhances the contribution to the visibility correlation arising from the emission of a single HI cloud. As changing $V$ does not affect the results very much, in this subsection we show the results for $V = 200\,\mathrm{km/s}$ only.

Figure 4 shows the results for $U = 300$. We find that the discrepancy between the linear, analytic predictions and the results of our simulations increases at larger values of $U$. Except at very small values of $\Delta\nu$, the simulated values are larger than the linear predictions. This is because the larger baselines probe smaller length scales
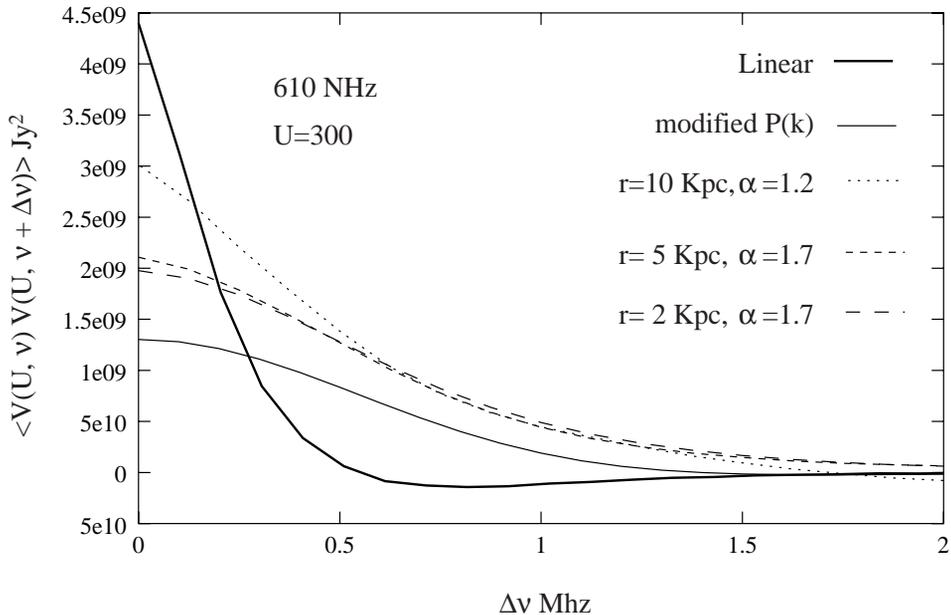
**Figure 4.** This is the same as Fig. 3 except that it shows results for $U = 300$.

which are significantly nonlinear (figure 1) and the amplitude of the fluctuations is larger than predicted by linear theory. At smaller scales the fluctuations are non-linear even in real space, and the modified formula (equation 7) based on only redshift space considerations grossly underestimates the visibility correlations. An important point is that at larger values of $U$ the visibility correlations calculated in the simulations do not fall as sharply with increasing $\Delta\nu$ as predicted in the linear calculations. In Paper c we found that the visibility correlations decay as $\propto \exp[-\Delta\nu/K]$, where the decay constant varies as $K \propto U^{-0.8}$ i.e., the decay is faster at larger baselines. Our simulations show that the decay with increasing $\Delta\nu$ is slower than predicted using linear theory. This is a consequence of the fact that the density fluctuations are non-linear on the length-scales being probed at these baselines. Another point to note is that the dependence on the parameters $R$ and $\alpha$, becomes relatively more pronounced at large values of $U$.

### 3.2  *325 MHz*

A point which should be mentioned right at the start is that at 325 MHz we are restricted in the values of $R$ for which we are able to carry out simulations. At 325 MHz the simulation volume is pretty large (table 1) and for $R = 2$ Kpc the total number of HI clouds in the simulation volume becomes too large for our computational resources. Also, in this subsection we use $V = 100$ km/s in our simulations. Figure 5 shows the results for the visibility correlations at $U = 100$. The behaviour at smaller baselines is not very different. We find that for $\Delta\nu < 1$ MHz the predictions of the analytic, linear calculations (Paper c) are very close to the values obtained in the simulation
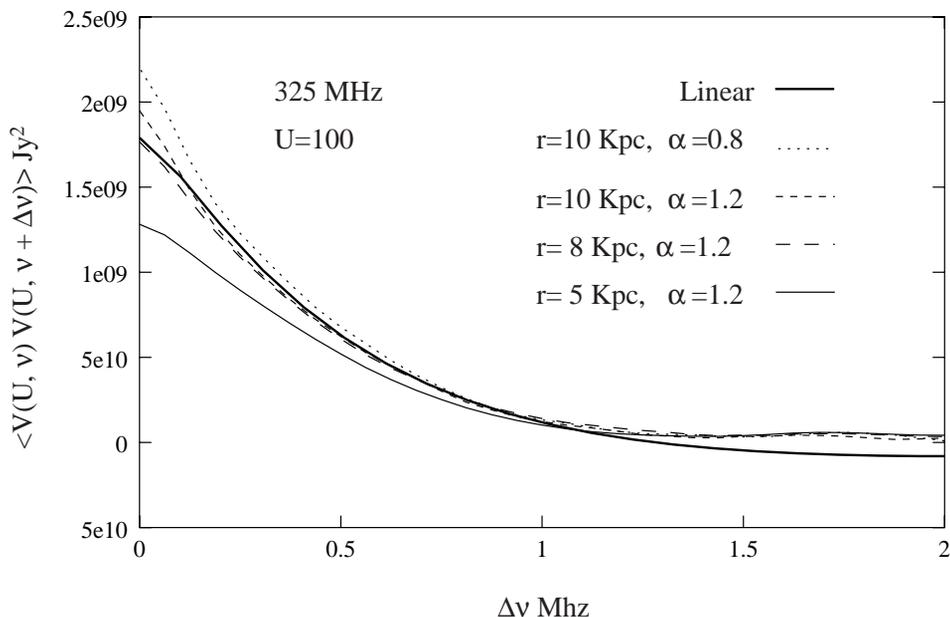
**Figure 5.** This shows the expected correlation between the visibilities $V(\mathbf{U}, \nu)$ and $V(\mathbf{U}, \nu + \Delta\nu)$ at the same baselines at two different frequencies. The rotational velocity of the HI disk is assumed to be $V = 100\,\text{km/s}$. The other parameters of the HI distribution take on values shown in the figure. These results are for the 325 MHz band.

for $r = 8\,\text{Kpc}$ and $\alpha = 1.2$. The results of the simulation are slightly larger than the analytic predictions when $r = 10\,\text{Kpc}$, and they are somewhat smaller than the analytic predictions at $r = 5\,\text{Kpc}$. For $\Delta\nu > 1\,\text{MHz}$ the results of the simulation are the same for all the parameters, and the value is slightly more than the analytic prediction. The power spectrum (Fig. 2) is in the linear regime at the Fourier modes which contribute to the visibility correlations at $U = 100$. The discrepancy between the analytic predictions and the results of our simulations can be attributed to a combination of the two factors discussed earlier:

(1) the effect of random motions on the redshift space clustering and
(2) correlations between the HI emission from the same cloud at different frequency channels.

Figure 6 shows the visibility correlations at $U = 400$. We find that the behaviour of the visibility correlations does not change very much for baselines in the range $100 < U \leq 400$. The power spectrum (Fig. 2) starts getting non-linear at Fourier modes corresponding to $U = 400$, but the effect is not very significant.

## 4. Discussion and conclusions

We take up for discussion two issues pertaining to the way we have modeled the distribution of HI clouds. First is our assumption that the HI clouds responsible for damped Lyman-$\alpha$ absorption lines are rotating disks, all with the same radius and
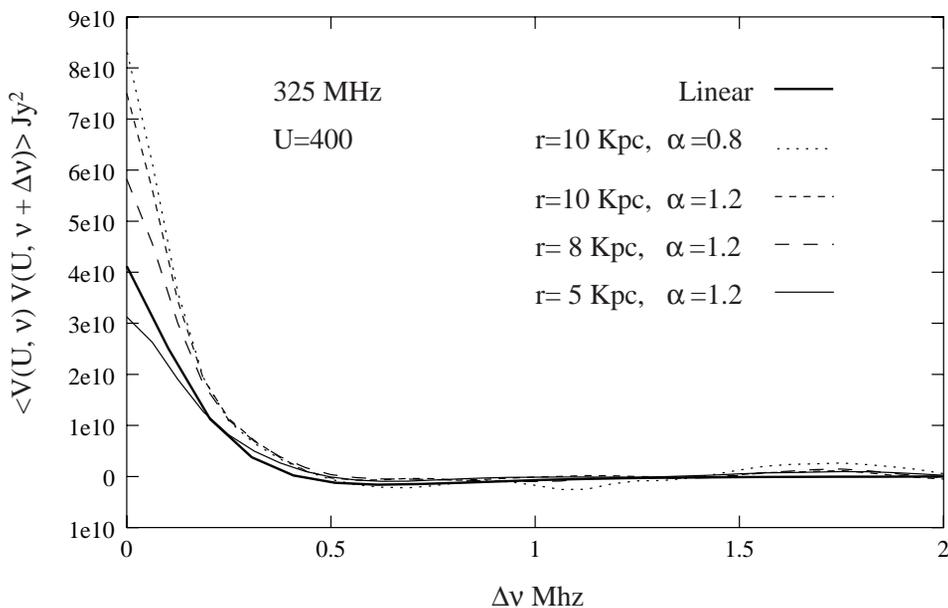
**Figure 6.** This is the same as Fig. 5 except that it shows results for $U = 400$.

rotational velocity. Prochaska and Wolfe (1998) have proposed that these HI clouds are the gaseous progenitors of present day galaxies. They have attempted to explain the observed kinematic of the damped Lyman-$\alpha$ absorption lines using a thick, rotating disk model for the HI clouds. Another model (Haehnelt *et al.* 1998) proposes that the observations could be better explained by modeling the absorption systems as protogalactic gas clumps undergoing merger. The second issue is our assumption that the HI column densities have a power law distribution and our choice of the value of the index $\alpha$. Lanzetta *et al.*(1991) show that the column density distribution at $z \simeq 2.5$ can be described by a power law with $\alpha \simeq 1.7$. In a later paper Lanzetta *et al.* (1995) show that the column density distribution evolves quite strongly with redshift, there being a tendency toward more high column density clouds at higher redshifts. In our work we have run simulations for two values of the index i.e., $\alpha = 1.2$ and 1.7. Having very briefly reviewed some of the prevalent views and having compared our assumptions with them, we note that our simulations seem to indicate that the visibility correlation signal does not depend very critically on the details of the properties of the HI clouds. We find that the visibility correlation signal has contribution from mainly two effects:

(1) correlations caused by the emission from the same cloud to different frequency channels, and
(2) the clustering of the clouds in redshift space.

The first effect is seen in the correlation at small values of $\Delta\nu$, where $\Delta\nu$ is smaller than the width of the HI line from an individual cloud. This effect manifests itself as a rise in the visibility correlations at small values of $\Delta\nu$ ($< 0.5$MHz). This effect is enhanced if the HI is distributed in a few clouds with large HI masses as compared to

the situation where the HI is in many small clouds with low HI masses. This seems to be the only effect of the fact that the HI is distributed in discrete HI clouds and is not continuously distributed. This is also the only place where the details of the HI distribution affects the visibility correlation.

We next turn our attention to the contribution to the visibility correlation signal from the clustering of the HI clouds. We may take the results for the visibility correlations at the values of the parameters $R$ and $\alpha$ where $N_{\mathrm{clouds}}$ is maximum as representing the results when the discrete nature of the HI distribution can be neglected (continuum limit). This assumption is justified at 610 MHz where there is very little difference in the results between $R = 5$ Kpc and $R = 2$ Kpc. We have not carried out simulations for $R < 5$ Kpc at 325 MHz, and simulations with smaller values of $R$ are needed at this frequency before we can be sure that the results for $R = 5$ Kpc really represent the continuum limit. Let us first discuss the results at the baselines for which the visibility correlation probes the power spectrum at length-scales which are in the linear regime. This is true for baselines with $U \leq 100$ at 610 MHz (Fig. 1). At 325 MHz most of the baselines which we have studied probe the power spectrum in the linear regime (Fig. 2). For all these baselines we find that the simulated values are less than the predictions of linear theory at small $\Delta\nu$ and the simulated values are larger than the linear predictions at large $\Delta\nu$. The transition occurs in the range $\Delta\nu \sim 0.5 - 1$ MHz. We propose that this discrepancy is a consequence of the fact that the fluctuations in the HI distribution in redshift space may be non-linear even on length-scales where linear theory holds in real space. This can be modeled by incorporating the effect of random peculiar velocities on the redshift space HI distribution. We show that including this effect gives a good fit to the simulated results at $U = 100$ for 610 MHz. At larger baselines the visibility correlation probes the power spectrum on length-scales where it is non-linear. Non-linear effects start influencing the visibility correlation at baselines $U \geq 200$ for 610 MHz, and these effects are very significant by $U = 400$. As a consequence of these effects the simulated visibility correlations do not fall off with increasing $\Delta\nu$ as quickly as predicted by linear theory. Also, the simulated values are larger than the linear predictions everywhere except at very small values of $\Delta\nu$. The range of $\Delta\nu$ where the simulated values are less than the linear predictions decreases with increasing $U$.

In conclusion we note that the HI signal predicted by our simulations are not drastically different from the analytic predictions presented earlier. In this paper we have been able to address the effects of the discrete nature of the HI distribution and the non-linear nature of the HI fluctuations in redshift space. We now have the tools necessary to simulate the HI signal expected at the GMRT. A full simulation of a GMRT observation requires us to also include the system noise as well as various galactic and extragalactic radio sources. Only then will we be able to make definite predictions as to whether it will be possible to detect the HI signal or not. Work is currently underway on this. The preliminary results indicate that it will be possible to have a $5\,\sigma$ detection at 610 MHz with one thousand hours of observation.

## References

Bagla, J. S., Nath, B., Padmanabhan, T. 1997, *MNRAS*, **289**, 671.

Bagla, J. S., White, M. 2002, astro-ph/0212228.

Ballinger, W. E., Peacock, J. A., Heavens, A. F. 1996, *MNRAS*, **282**, 877.

Bharadwaj, S., Nath, B., Sethi, S. K. 2001, *JAA*, **22**, 21.

Bharadwaj, S., Sethi, S. K. 2001, *JAA*, **22**, 293.

Bharadwaj, S., Pandey, S. K. 2003, *JAA*, **24**, 23.

Brainerd, T. G., Bromley, B. C., Warren, M. S., Zurek, W. H. 1996, *Ap. J.*, **464**, L103.

Bromley, B. C., Warren, M. S., Zurek, W. H. 1997, *Ap. J.*, **475**, 414.

Bunn, E. F., White, M. 1996, *Ap. J.*, **460**, 1071.

Efstathiou, G., Bond, J. R., White, S. D. M. 1992, *MNRAS*, **250**, 1p.

Fisher, K. B., Davis, M., Strauss, M. A., Yahil, A., Huchra, J. P. 1994, *MNRAS*, **267**, 927.

Haehnelt, M. G., Steinmetz, M., Rauch, M. 1998, *Ap. J.*, **495**, 647.

Kaiser, N. 1987, *MNRAS*, **227**, 1.

Kumar, A., Padmanabhan, T., Subramanian, K. 1995, *MNRAS*, **272**, 544.

Lanzetta, K. M., Wolfe, A. M., Turnshek, D. A., Lu, L. 1991, *Ap. JS.*, **77**, 1.

Lanzetta, K. M., Wolfe, A. M., Turnshek, D. A. 1995, *Ap. J.*, **430**, 435.

Peacock, J. A., Dodds, S. J. 1994, *MNRAS*, **267**, 1020.

Peebles, P. J. E. 1980, *The Large-Scale Structure of the Universe*, (Princeton: Princeton University Press)

Péroux, C., McMahon, R. G., Storrie-Lombardi, L. J., Irwin, M. J. 2001, *MNRAS*, **346**, 1103.

Prochask, J. X., Wolfe, A. M. 1998, *Ap. J.*, **507**, 113.

Saini, T., Bharadwaj, S., Sethi, K. S. 2001, *Ap. J.*, **557**, 421.

Storrie–Lombardi, L. J., McMahon, R. G., Irwin, M. J. 1996, *MNRAS*, **283**, L79.

Subramanian, K., Padmanabhan, T. 1993, *MNRAS*, **265**, 101.

Sunyaev, R. A., Zeldovich, Ya. B. 1975, *MNRAS*, **171**, 375.

Suto, Y., Suginohara, T. 1991, *ApJL*, **370**, L15.

Swarup, G., Ananthakrishan, S., Kapahi, V. K., Rao, A. P., Subrahmanya, C. R., Kulkarni, V. K. 1991, *Curr. Sci.*, **60**, 95.

Weinberg, D. H., Hernquist, L., Katz, N. S., Miralda-Escude, J. 1996, *Cold Gas at High Redshift* (eds.) M Bremer, H Rottgering, C Carilli and P van de Werf, (Dordrecht: Kluwer)